The citation for this article is Mallama, A., Stockdale, C., Kroubsek, B., and Nelson, P. (2010) *Icarus* **210** 346–357. DOI 10.1016/j.icarus.2010.06.007

Assessment of the Resonant Perturbations Errors in Galilean Satellite Ephemerides Using Precisely Measured Eclipse Times

Abstract

Astrometric satellite positions are derived from timings of their eclipses in the shadow of Jupiter. The 548 data points span 20 years and are accurate to about 0.006 arc seconds for Io and Europa and about 0.015 arc seconds or better for Ganymede and Callisto. The precision of the data set and its nearly continuous distribution in time allows measurement of regular oscillations with an accuracy of 0.001 arc second. This level of sensitivity permits detailed evaluation of modern ephemerides and reveals anomalies at the 1.3 year period of the resonant perturbations between Io, Europa and Ganymede. The E5 ephemeris shows large errors at that period for all three satellites as well as other significant anomalies. The L1 ephemeris fits the observations much more closely than E5 but discrepancies for the resonant satellites are still apparent and the measured positions of Io are drifting away from the predictions. The JUP230 ephemeris fits the observations more accurately than L1 although there is still a measurable discordance between the predictions and observations for Europa at the resonance period.

Key words: Orbit determination, Io, Europa, Ganymede, Callisto

1. Introduction

Satellite orbit theories have numerous important applications including geophysical studies of the moons and their planets. A universally recognized example is the tidal interaction between the Earth and the Moon. Eclipses of satellites by their planets provide important data for orbit theories and some geophysical information can be derived immediately from eclipse observations themselves. For example Neugebauer et al., 2005 measured the thermal inertia of Iapetus based on observations obtained at 20 and 2.2 μm when that satellite was in the shadow of the saturnian ring system. Additionally, the state of a planetary atmosphere can be assessed from photometry of satellite eclipses. Mallama et al., 1995 deduced the altitude of atmospheric fall-out from the impact of comet Shoemaker-Levy 9 with Jupiter, Nicholson et al., 1997 found that methane absorption rather than refraction was the principal cause of satellite dimming during 2.3 μm observations of the saturnian satellites during eclipses, and Mallama et al., 2000b determined the altitude of the haze layer at the north and south poles of Jupiter from partial eclipses of the satellite Callisto. In addition to geophysics, accurate theories are essential in the production of ephemerides for navigating interplanetary spacecraft. Satellite positions must be especially precise for close range remote sensing and during fly-bys used in gravity assists.

The astrometric results in this paper were derived by fitting photometric ingress or egress eclipse data to a synthetic light curve which is generated using a physical model. Section 2 describes the model, which accounts for the effects of the Sun-Jupiter-Earth-satellite geometry, refraction of sunlight in the atmosphere of Jupiter, and the bi-directional reflectance (BDR) functions of the satellites. Some refinements to the model first developed by Mallama, 1991 and 1992 are reported. The procedures for fitting the synthetic light curve to observed photometry and that of deriving event mid-times are also discussed. The method of observation is described in Section 3 and a listing of mid-event timings that span 20 years is given. The procedure for deriving residuals between these observations and ephemeris calculations is explained and the overall methodology

is validated. The differences between the along-track satellite *observed* positions and those *calculated* (that is, *O – Cs)* with the JUP230 ephemeris of Jacobson et al., 1999 (and later work), the L1 ephemeris of Lainey et al., 2004a, 2004b and 2006, and the E5 ephemeris of Lieske, 1998 are evaluated in Section 4. In Section 5 regular O – C oscillations are characterized and identified with the resonant perturbations between Io, Europa and Ganymede. Section 6 concludes with estimation of the uncertainties in the astrometric data.

2. Photometric Eclipse Model

Astrometric information is derived from eclipse photometry by means of a model based on the geometry between the Sun, satellite, planet and observer, as well as two physical factors. The first of these is refraction of rays from the Sun, occurring about 150 km above the clouds at the planetary limb, which causes the dimming of sunlight that is observed during an eclipse. Atmospheric refraction must be integrated with the geometrical configuration in order to calculate the intensity of light that impacts a grid of points on the satellite surface. The other factor is the satellite BDR function which determines how much light from each of the grid of points is directed to the observer. The BDR depends on the distribution of satellite albedo features and on limb darkening. The center-of-figure of a Galilean satellite is usually offset from its photocenter by 100 km or more, so the effect has about the same magnitude as does refraction.

The model is used to generate a synthetic light curve tailored to the geometry of the observed ingress or egress. Atmospheric refraction, which is fixed in the model, acts on sunlight bound for the satellite according to the geometry of the Sun, planet and satellite. The BDR, which is also fixed, allows for computation of the intensity of light reflected toward the observer; so it depends on the geometry of the Sun, satellite and observer.

2.1 Atmospheric refraction

The dimming of sunlight is caused by differential refraction in the milli-bar (mbar) pressure domain of the atmosphere where rays are bent inward toward the planet center. The intensity of light traversing the atmosphere at lower altitudes becomes fainter because refraction increases progressively with atmospheric density, which is exponential. The diminished strength of any refracted ray at the satellite location can be computed from Eq. 1 (Baum and Code, 1953)

$$\varphi_0 / \varphi_r - 2 + \ln (\varphi_0 / \varphi_r - 1) = d_0 - d$$

(Eq. 1)

where φ_r / φ_0 is the ratio of that intensity to its full intensity before refraction and the differential distance $d_0 - d$ is measured in atmospheric scale heights. The special case where $d - d_0 = 0$ and $\varphi_r / \varphi_0 = 0.5$ is illustrated by the path of this half-intensity ray from the Sun to the satellite in Fig. 1 and relates to the radius of curvature, *a*, in Eq. 2 below. The half-intensity ray strikes the satellite at the location in space that defines the half-phase of an eclipse ingress or egress.

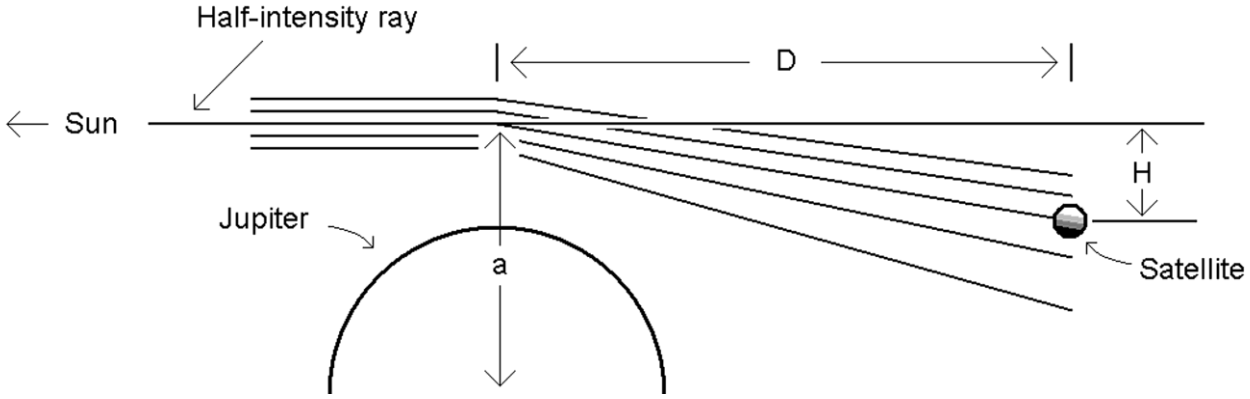

Fig. 1. Differential refraction in the planetary atmosphere reduces the intensity of light from the Sun, and the ray diminished to half-intensity is shown impacting the middle of a satellite. The symbols are used in the text to define the bending angle and the radius of this ray.

The minimum altitude of the half-intensity ray for Io is taken from a study by Spencer et al., 1990 where it is reported to be at the 2.2 mbar pressure level or 133 km above the one-bar level. The altitudes for the other satellites were derived relative to Io from Eq. 2, which is also from Baum and Code and is illustrated by Fig. 1.

$$\theta = H / D = v\,(2\pi a/H)^{0.5} \qquad \text{(Eq. 2)}$$

where angle of deflection, θ, is determined geometrically by the atmospheric scale height, H, divided by the distance from the planetary limb to the satellite, D. Physically, the ray is bent by atmospheric gas for which the refractivity is v, at the radius a, mentioned above. The minimum altitudes of the half-intensity rays for Europa, Ganymede and Callisto are thus found to be 145, 160 and 172 km, respectively.

2.2 Integrated luminosity

The total luminosity at any location within the planetary shadow is a summation over the intensity of all rays from the solar disk that impact on that point. In the geometrical case of a planet with no atmosphere there will be a completely dark umbral region corresponding to locations where a straight line to the Sun intersects the planet. The umbra is surrounded by a penumbral annulus, wherein a portion of the solar disk is visible, and which corresponds in width to the apparent diameter of the Sun projected from the planet limb to the satellite distance. The computation of luminosity in the geometric penumbra is straightforward although there is a minor effect from solar limb-darkening. The dashed line in Fig. 2 shows luminosity increasing from zero at the boundary between the umbra and penumbra to unity at the outer edge of the penumbra during an egress.

For a planet with an atmosphere, however, luminosity in the shadow is a summation over products of limb-darkened solar intensity times the effect of refraction as computed from Eq. 1. In this case the full uneclipsed luminosity for the satellite is attained a short distance outside of the geometric penumbral boundary, and significant brightness penetrates a long distance inside of the umbral boundary due to refraction as shown by the solid line in Fig. 2. The graph also shows that the luminosity at phase 0.5 is substantially greater than half even though that location is defined by the projection of a half-intensity ray from the center of the solar disk.

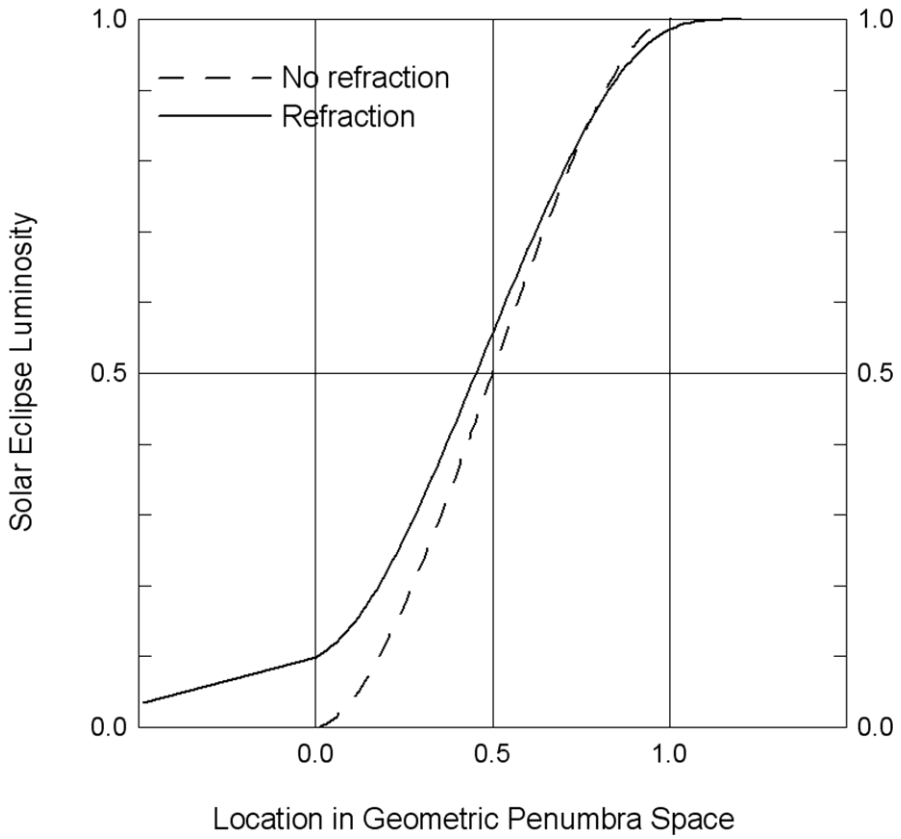

Fig. 2. The normalized luminosity of the Sun sensed at the distance of Io from the limb of Jupiter as a function of position, which is defined geometrically as the umbra ($X < 0$) and the penumbra ($0 < X < 1$). Zero and unity luminosity for the case of no refraction correspond with these geometric boundaries, but when refraction is taken into account the curve extends inside and outside of the penumbra. A half-intensity ray from the center of the solar disk falls at 0.5 on the horizontal axis.

2.3. Satellite characteristics

In addition to the solar eclipse luminosity described above, the physical size and the BDR characteristics of a satellite are taken into account when computing its integrated brightness in the planetary shadow. The details of BDR functions adopted for the Galilean satellites are listed by Mallama, 1991. The albedo differences between the leading and trailing hemispheres of these satellites result in significant offsets between their centers-of-luminosity and centers-of-figure. When combined with limb-darkening and phase effects the total offsets are hundreds of km and

their exact size and direction depends on the geometry of the eclipse event and the viewing angle from Earth.

The BDR model for Callisto was modified after the results in Mallama et al., 2000a were published. The leading/trailing hemisphere albedo component of the BDR function for that satellite used in the original eclipse model was based on an incorrect interpretation of the photometric results for its surface reported by Buratti, 1991 and Squyers and Veverka, 1981. After discussion with Buratti (private communication, 2002) the eclipse model BDR was corrected by changing the distribution of brightness as a function of the angle, ρ, which is measured along the satellite surface from the apex of its orbital motion. Specifically, the coefficient of cos(ρ) given in Mallama, 1991 was changed to +0.057. The original model resulted in observed timings that were consistently too early relative to ephemeris predictions, while the corrected model resolves these systematic differences as reported in Section 4.4 of this paper.

2.4. The synthetic light curve and the method of fitting observations

The brightness of a satellite is evaluated as a function of its changing position in the solar eclipse region during ingress or egress. This results in the synthetic light curve for a particular event. That brightness at any one location is computed by integrating the product of solar eclipse luminosity and the BDR function over the hemisphere of the satellite facing the sensor. Satellite eclipse phase space is a useful construct defined such that phase zero of an egress corresponds to the leading edge of the satellite crossing from the geometric umbra into the penumbra and phase one occurs when its trailing edge exits the geometric penumbra, and vice-versa for an ingress. While half-phase in eclipse space corresponds with that shown in Fig. 2 for geometric penumbra space, the limits at phases zero and unity are extended because of the finite radii of the satellite.

In order to correctly represent the geometry of an event the solar phase angle and the angle at which the shadow crosses the globe of the satellite are input to the model. Figures 3 and 4 demonstrate synthetic egress light curves for variations of phase angle and satellite.

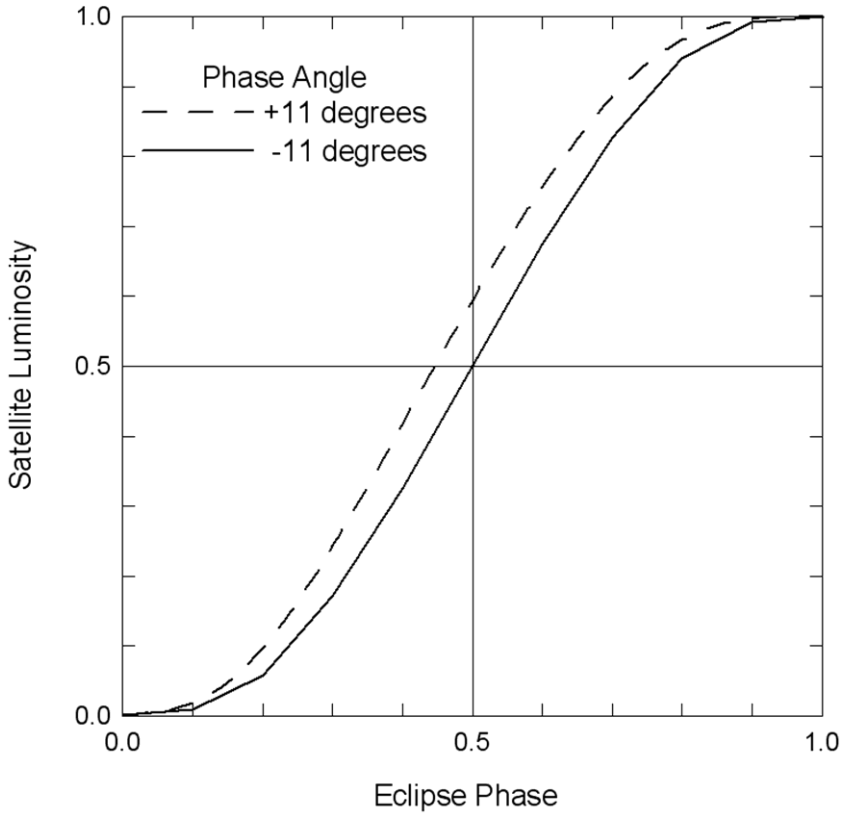

Fig. 3. The brightness of a satellite during an eclipse depends on phase angle, which is taken to be negative before the opposition of Jupiter from the Sun and positive afterward. In these synthetic egress light curves Ganymede attains half-luminosity at phase 0.499 when the event occurs at phase angle -11 degrees or morning quadrature with the Sun. However, the same luminosity is attained at phase 0.446, which is 36 seconds of time earlier for an event at evening quadrature. That difference is for eclipses that occur at the equator of Jupiter, but it can exceed one minute when the eclipse latitude is farther from the equator.

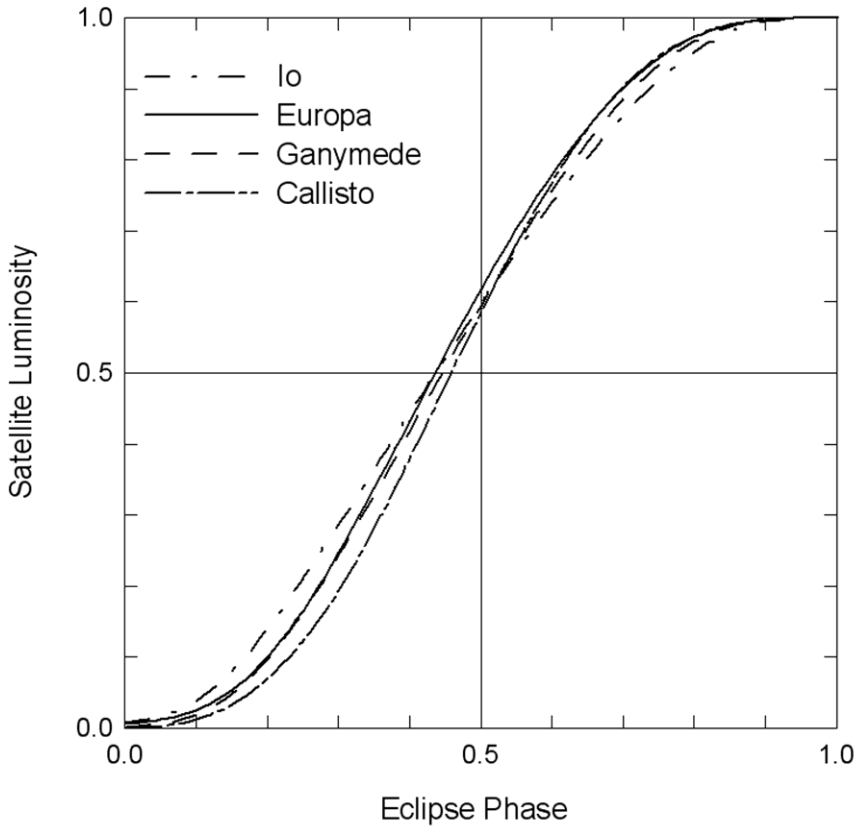

Fig. 4. Differences between synthetic light curves for the Galilean satellites are evident even when they are evaluated at the same phase angle, +11 degrees in this case. BDR characteristics, Sun-planet-moon geometry, and refraction contribute to the variation. Notice, too, that the luminosity at phase zero is near zero and that at phase one is near unity, in contrast to the solar eclipse luminosity with refraction shown in Fig. 2. This is due to the large size of the satellites relative to the width of the penumbral shadow.

Model luminosities are fitted to photometric data in order to establish distances between the center of the satellite and planet in the plane of the sky as seen from the Sun as a function of time. The fitting process for light curves is a non-linear least squares problem of the type described by Bevington, 1969. The model is parameterized and successive iterations adjust the parameters until the differences between modeled and observed data are reduced to a minimum. For astrometric purposes the critical parameter is the time of half-phase, which can be compared with that predicted by an ephemeris. The luminosity scale and the time scale are also adjusted.

3. Observation and Validation

CCD recordings of Galilean satellite eclipses began in 1990 when solid state sensors had become widely available. Older visual timings spanned more than three centuries, however they were very imprecise. Photoelectric photometry did not greatly improve the precision because the steep non-linear sky background near the limb of Jupiter introduced large biases into the satellite luminosity measurements. However, the linear two dimensional photometric data from a CCD chip proved to be ideal because the sky background could be accurately isolated and removed. This section begins by describing how the raw CCD images were acquired and how photometric data were extracted from them. Next, a listing of all the half-phase timings is presented, and finally the eclipse model and data analysis techniques are validated.

3.1 Observational methods, photometric analysis and timing results

A standard procedure has been followed during the 20 years of observation reported here. The eclipses were recorded through V-band filters with telescopes ranging from 20 to 40 cm in aperture and from 2 to 5 m in focal length. Typically about 100 images were taken during an event and each image was time tagged based on a clock synchronized to WWV radio broadcasts, GPS satellites signals, NTP Internet sources or the NIST telephone service.

The data were analyzed with customized aperture photometry software that produces accurate satellite luminosities even in the vicinity of the bright nearby planet. Precise sky background subtraction was accomplished by reading data from a tailored annulus centered around the measurement aperture for the satellite. The brightest 25% and the faintest 25% of the luminosities in the annulus were rejected, thus masking out the sky in the directions toward and away from Jupiter where the gradient is steepest. The remaining 50% of the luminosity data represents the sky background brightness at the same distance from the planetary limb as the satellite. The

observed normalized brightness of a satellite when totally eclipsed is generally within 1% of zero, which demonstrates the accuracy of the sky subtraction.

Additionally, each CCD image of the eclipsing satellite contains at least one other moon for luminosity and positional reference. The analysis program uses the locations of the two satellites and their relative motion over the course of the event to track the eclipsing satellite even when it is very faint or totally eclipsed.

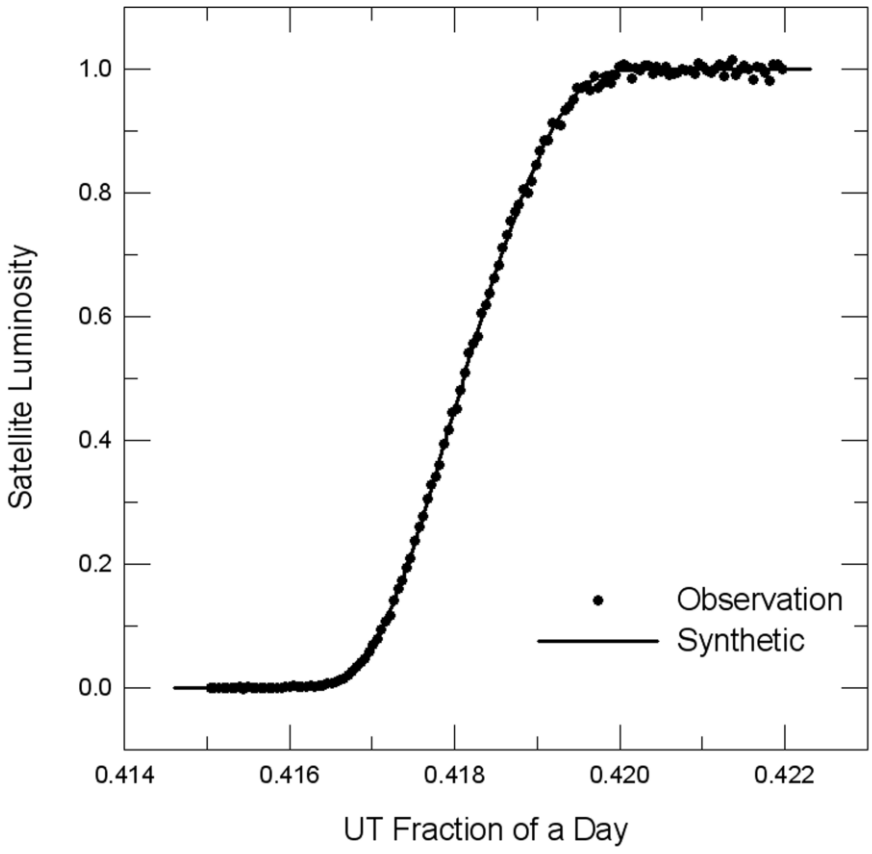

Fig. 5. An egress of Europa observed on 2007 July 30 demonstrating the close fit between photometric data and the synthetic light curve.

The resulting set of luminosities for each ingress or egress is fitted to a synthetic light curve (customized for that event) by the non-linear technique described in Section 2.4 and illustrated in Fig. 5. The observed times of half-phase in seconds measured from the epoch of J2000 are listed in Table 1 where the satellites are identified by numbers 1 through 4 for Io, Europa, Ganymede and Callisto, respectively, and eclipse Ingress or Egress is indicated by I or E.

The data in Table 1 are the basis of this paper and its most important result, so the following example is given in order to clearly specify the contents. The first timing with a positive number of seconds, 470546.0, corresponds to half-phase of an event that occurred on 2000 January 6 at 22:41:21.8 UTC, which was 470481.8 s later than 2000 January 1.5 UTC. The difference of 64.2 s between the numbers quoted above corresponds to the offset between UTC and ephemeris time (ET) at that epoch. The quantity '2E' in this same record of the Table indicates that it was an egress 'E' of the satellite Europa '2'. Please contact the first author for information about using the eclipse timings as astrometric data.

Table 1 is at the end of the manuscript

3.2 Validation by comparison with the dimensions of Jupiter

The long time span and the large number of observations in this study allow the consistency of the observing, modeling and fitting techniques to be verified. In particular, the absolute accuracy can be assessed by comparing satellite positions computed at the times of half-phase with the location of Jupiter's limb. While discrepancies for any one event are to be expected because of ephemeris and observational uncertainties, the satellite and limb positions should correspond when the whole data set is averaged.

Three ephemerides are used to perform this validation and are referenced throughout the remainder of this paper. JUP230 is the final ephemeris for the Galileo satellite mission. Jacobson

et al., 1999 described the early orbit modeling work that centered on Galileo spacecraft data beginning in 1995 and eventually extending through 2003. JUP230-Long gives the same results as JUP230 but it allows computations for years before 2000.0 and the two are considered equivalent here. The L1 theory of Lainey et al., 2004a and 2004b fits a long time span of observations, beginning with astrographic observations in 1891. The E5 ephemeris (Lieske, 1998) is an analytical model that had been the state of the art before JUP230 and L1 were developed using numerical integration.

These ephemerides were used to calculate satellite positions at the observed ET corrected for the light-time between the satellite and the Earth. The position of Jupiter relative to the satellite was projected to the heliocentric plane of the sky as depicted in Fig. 6. Then the radial distance between the centers of Jupiter and the satellite in that plane was determined, and this quantity is referred to as the satellite's ephemeris radial distance. Next the radius at the minimum altitude of the half-intensity ray, corrected for refraction, was subtracted from the ephemeris radial distance, and this is referred to as the delta radius. Since Jupiter is an ellipsoid, this minimum altitude is the one projected by the pole-tilted ellipsoid on the sky (also depicted in the figure).

The very small average delta radius values of -6.0 km (+/- 9.7) for JUP230, -23.8 (+/- 20.6) for L1 and -2.6 (+/- 6.8) for E5 validate the methodology. In the next section the individual delta radii corresponding to each of the Galilean satellites are used in the evaluation of the ephemerides.

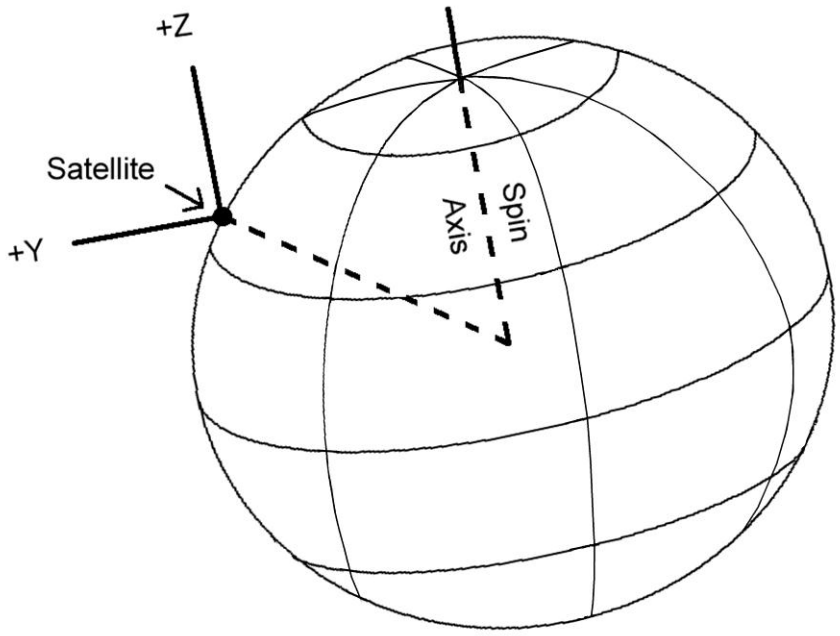

Fig. 6. The X-axis points out of the plane of this figure toward the Sun. The spin axis of Jupiter is in the XZ plane. The latitude at Jupiter's limb (indicated by the dashed line) that projects onto the satellite is derived from the arc tangent of Z / Y at the center of the planet. The radius of the ellipsoid at that point on the limb is computed from the latitude.

4. Characterization of the Eclipse Residuals

Satellite ephemeris errors are usually dominated by their along-track component because orbital perturbations act most strongly in that direction. Since the Galilean satellites tend to encounter Jupiter's shadow at a small angle of incidence the eclipses are very useful for evaluating along-track residuals. In particular, the eclipses of Io occur within 18 degrees of Jupiter's equator and those of Europa happen within 35 degrees. While the eclipses of Ganymede and Callisto can occur at higher latitudes they are still very effective for evaluating along-track error because the out-of-plane ephemeris uncertainties are much smaller.

Eclipse time O – Cs and distances are related by the common equation for velocity. If the event was an ingress and the O – C in time is positive, then the satellite was observed to be at half-phase when its ephemeris calculates a position closer to Jupiter, thus the delta radial distance (defined in the previous section) is negative. Conversely, for an egress, a positive O – C in time indicates a positive delta radius because the ephemeris indicates a satellite farther from Jupiter than the location of half-phase.

The average delta radius parameters for individual satellites are often significantly different from zero (though usually less than one percent of the satellite radius) as shown in Table 2. The non-zero averages are most likely due to a combination of uncertainties in the BDR model, the atmosphere model and the ephemerides. Therefore, in the following analysis, the delta radial distance for each event was corrected for the average delta radius of the appropriate satellite and ephemeris before the O – C was derived.

4.1. Io - oscillation and drift

The O – C residuals of Io plotted in Fig. 7 show that most timings of half-phase agree with predictions from all 3 ephemerides within about 5 s. The root-mean-square (rms) residuals range from a best of 2.0 s for JUP230 to 2.7 s for L1 to a worst of 3.7 s for E5 as indicated in Table 2.

The most striking signature in the residuals is a cyclic variation with a period near 1.3 years relative to the E5 ephemeris. Fig. 8 shows the correlation between O – Cs and sinusoids fitted to them as a function of period. The peak correlation is that at 1.28 years for E5 and there is a smaller one nearby at 1.31 for L1. The periods, amplitudes and phases for these oscillations and those of the other satellites are listed in Table 3. The other notable feature in the O – Cs is the drift of Io relative to the L1 ephemeris beginning in 2002. That model appears to be predicting eclipse times that are increasingly too late and by the end of 2009 the discrepancy was about 65 km.

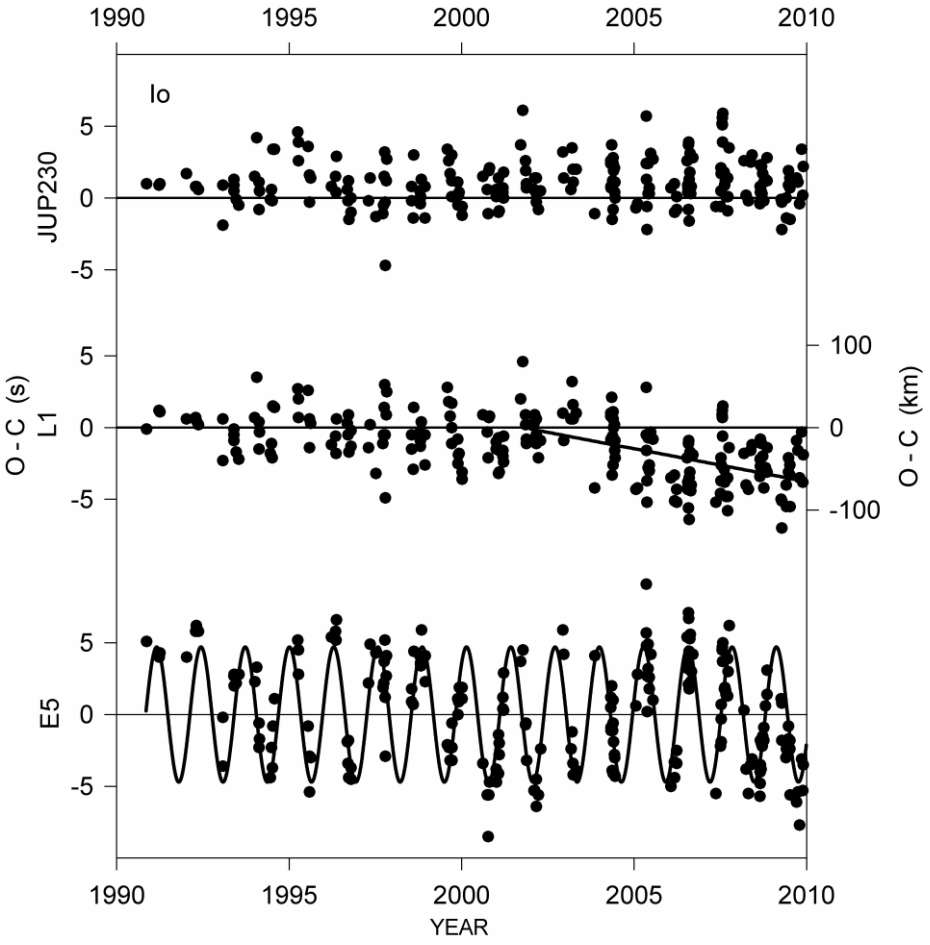

Fig. 7. The residuals between observed half-phase times for Io and calculations from the JUP230, L1 and E5 ephemerides. Those for E5 are fitted with a sine function having a period of 1.28 years. The trend line for L1 beginning in 2002 indicates that observed eclipse times are increasingly early relative to that ephemeris.

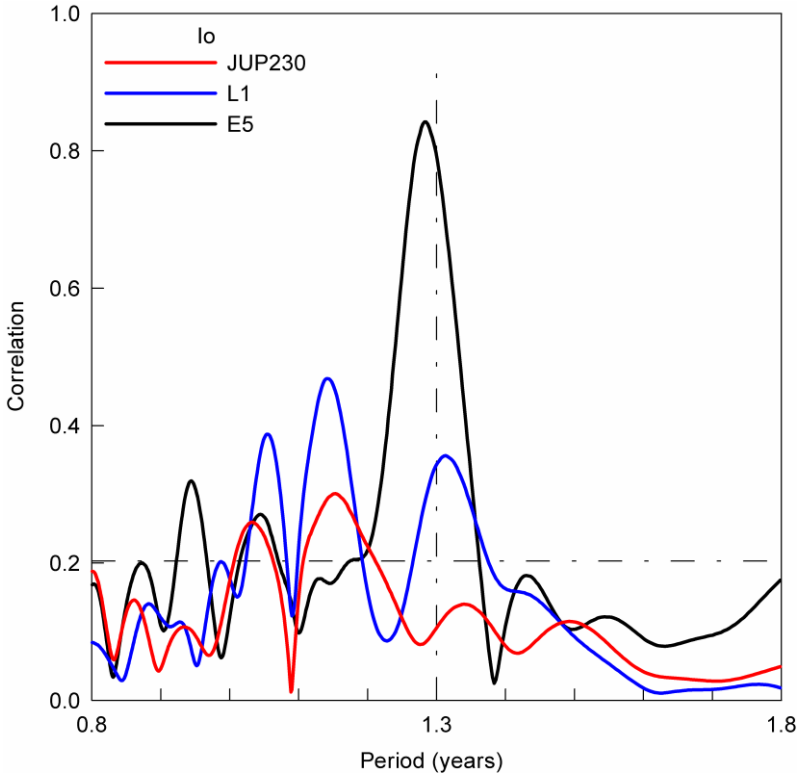

Fig. 8. The correlation between sine fits and the residuals of Io to JUP230, L1 and E5 for periods around 1.3 years. The dashed horizontal line indicates 99% confidence.

.

Table 2. Ephemeris evaluation summary

	JUP230	L1	E5
Io, 211 observations			
Average delta radius (km)	+9.6 (3.6)	-14.2 (5.3)	+20.2 (4.3)
O – C mean (s)	+1.1 (0.1)	-1.3 (0.1)	-0.7 (0.3)
O - Cs rms (s)	2.0	2.5	3.7
Europa, 149 observations			

Average delta radius (km)	+11.9 (3.2)	+20.8 (7.4)	+4.7 (20.4)
O – C mean (s)	-0.3 (0.2)	-0.7 (0.3)	-1.5 (1.6)
O - Cs rms (s)	2.0	3.9	19.0
Ganymede, 149 observations			
Average delta radius (km)	-25.1 (5.4)	-78.5 (8.9)	-41.2 (12.4)
O – C mean (s)	-3.6 (0.4)	+1.7 (0.7)	+2.7 (1.3)
O - Cs rms (s)	6.3	8.2	16.0
Callisto, 39 observations			
Average delta radius (km)	-20.4 (13.2)	-23.0 (13.7)	-7.0 (10.2)
O – C mean (s)	-3.0 (1.3)	+2.5 (1.5)	-2.2 (1.6)
O - Cs rms (s)	8.5	9.4	9.6

The numbers in parentheses are uncertainties.

4.2 Europa - large O – Cs

The residuals of Europa to E5 are more than 5 times as large as those of Io, with an overall rms of 19.0 s or 260 km. They are significantly negative in 1990, increase to a large positive value around the year 2000, and then turn negative again as shown in Fig. 9. This large error in the E5 ephemeris has been noted before by Lainey et al., 2004b and by Mallama et al., 2000a. The improvements of JUP230 and L1 are very evident from the graph. Since this long term variation adds complexity to the analysis of short period oscillations it was fitted with the empirical function shown by the dashed line in the graph. After this correction the remaining residuals fit a sine curve with period 1.27 years which is just 0.01 year less than that for Io. The correlation coefficient between the observations and the sinusoid for E5 is extremely high as shown in Fig. 10. There is

also a strong correlation near the same period for L1 and one that is weaker but still significant for JUP230.

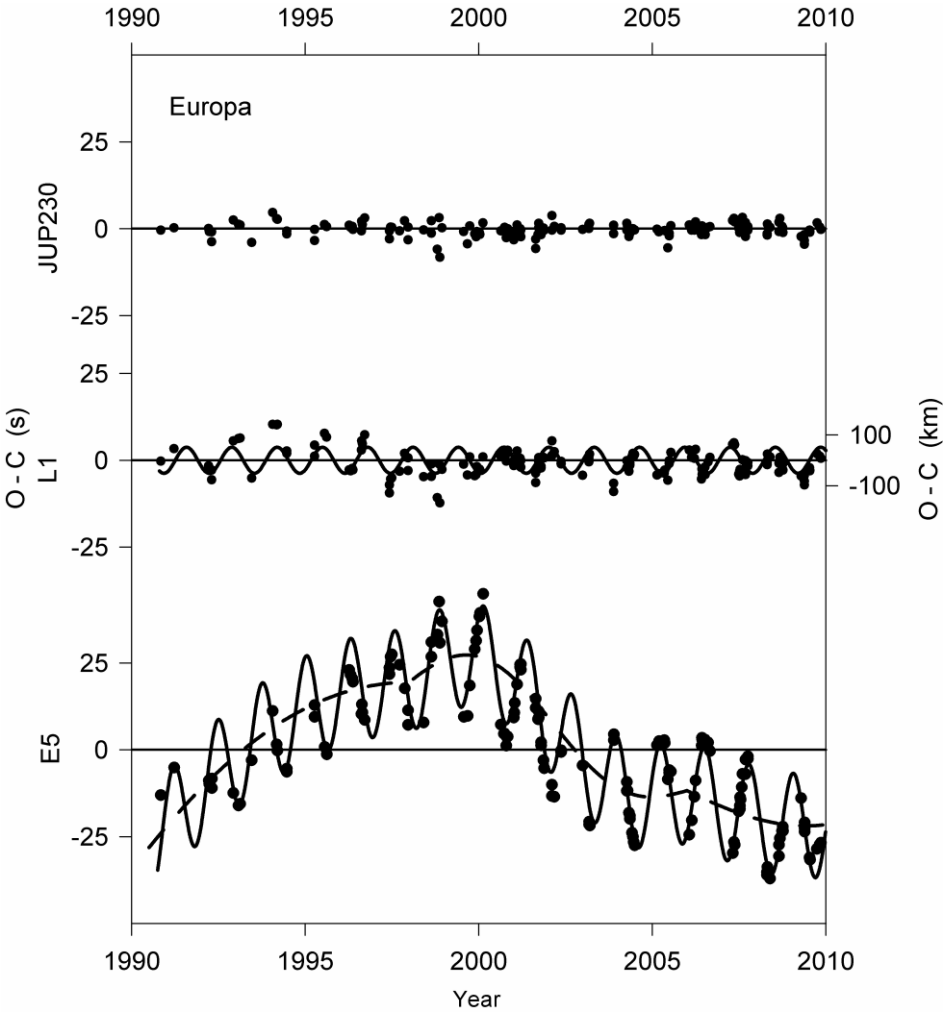

Fig. 9. When the long term O – C variations of Europa to E5 are removed with a heuristic function (dashed line) the 1.27 year sine term is very apparent. An oscillation of about the same period but smaller amplitude is evident for L1.

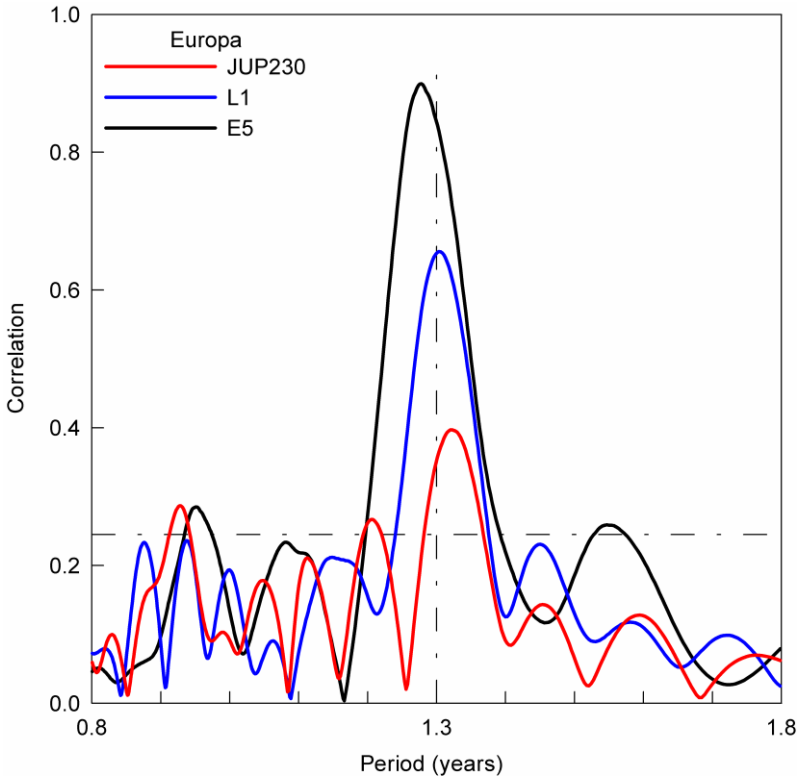

Fig. 10. The correlation between sine fits and the residuals of Europa to JUP230, L1 and E5. There are significant correlations for all 3 ephemerides at periods near 1.3 years.

.

4.3 Ganymede - drift and ephemeris biases

The residuals to E5 for Ganymede shown in Fig. 11 are scattered around zero until 2007 when a trend becomes evident. This behavior mirrors the plot in Fig. 6 of Lainey et al., 2004b which compares predictions of L1 with those of E5. The fit of the residuals to E5 shown by the sinusoid corresponds to a period of 1.30 years, so it is similar to those of Io and Europa. The E5 correlation is strong as shown in Fig. 12 while a peak for L1 just less than 1.3 years is weaker though still significant. The mean O – C values for Ganymede range from -3.6 for JUP230 to +1.7 for L1 and +2.7 for E5. This spread, which corresponds to 67 km, is the largest among the satellites.

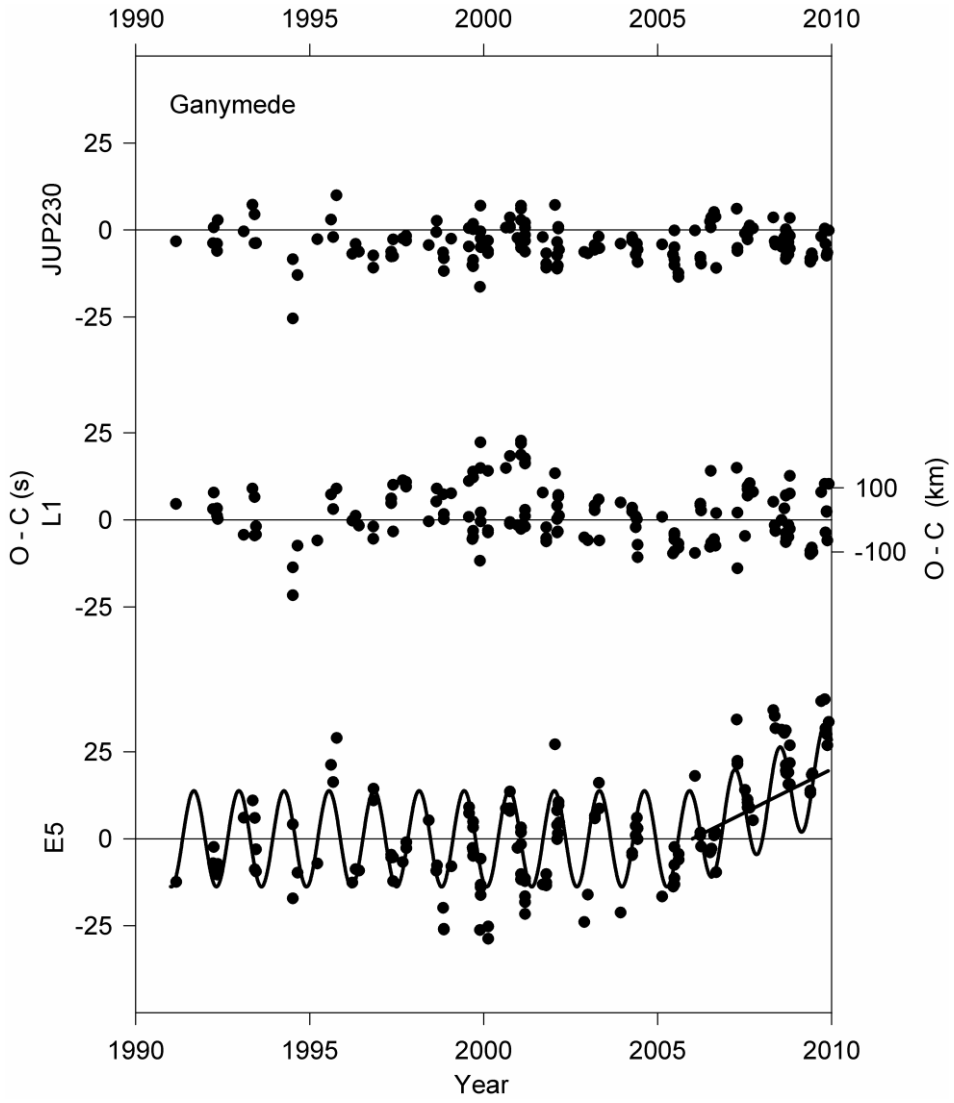

Fig. 11. The observed position of Ganymede has fallen behind that predicted by the E5 ephemeris in recent years as shown by the trend line. The L1 and JUP230 ephemerides predict eclipses more accurately although there is a considerable bias between them. The average eclipse timing is early relative to JUP230 and late relative to L1.

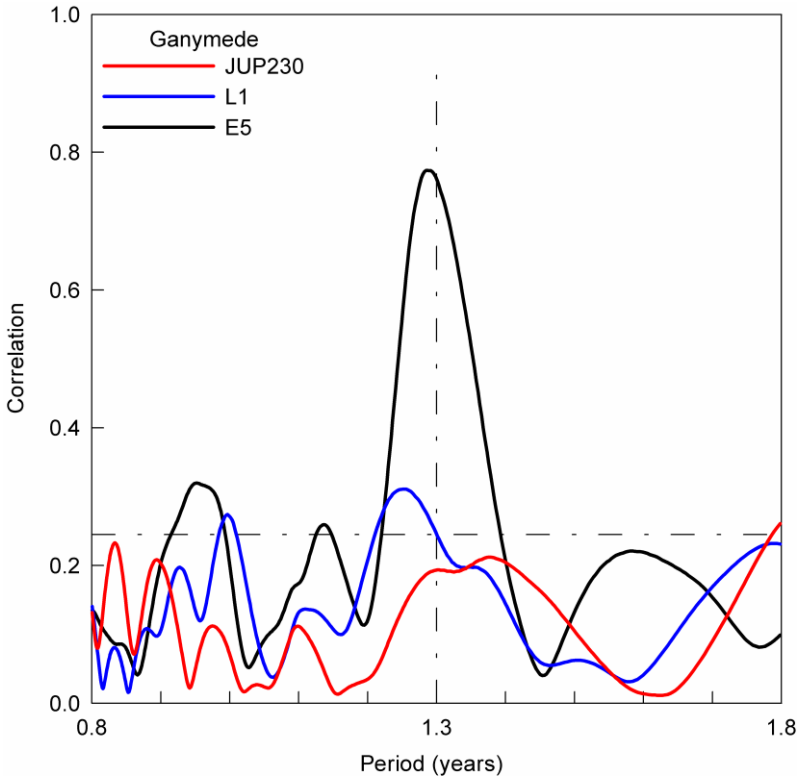

Fig. 12. The correlation between sine fits and the residuals for Ganymede to the three ephemerides.

4.4 Callisto - improved results

The leading/trailing hemisphere albedo parameter of the BDR function for Callisto given in the model paper by Mallama, 1991, and used for analysis of the results reported by Mallama et al., 2000a, has been corrected as described in section 2.3. Consequently, the observed times of half-phase that had appeared to be systematically much too early relative to E5 (open circles in Fig. 13) are now far more consistent with it (filled circles). While the previously negative bias revealed the error in the old BDR, the parameterization was not adjusted empirically to make the data fit the ephemeris; rather the new albedo parameter was derived from the corrected understanding of the BDR. So, the better overall fit between ephemeris theory and observations is an independent verification of the corrected satellite model. The O – Cs for E5 in the most recent years seem to be

trending negatively while those for JUP230 and L1 remain scattered around zero. Fig. 14 does not indicate high correlations between O – Cs and sine fits for any of the ephemerides.

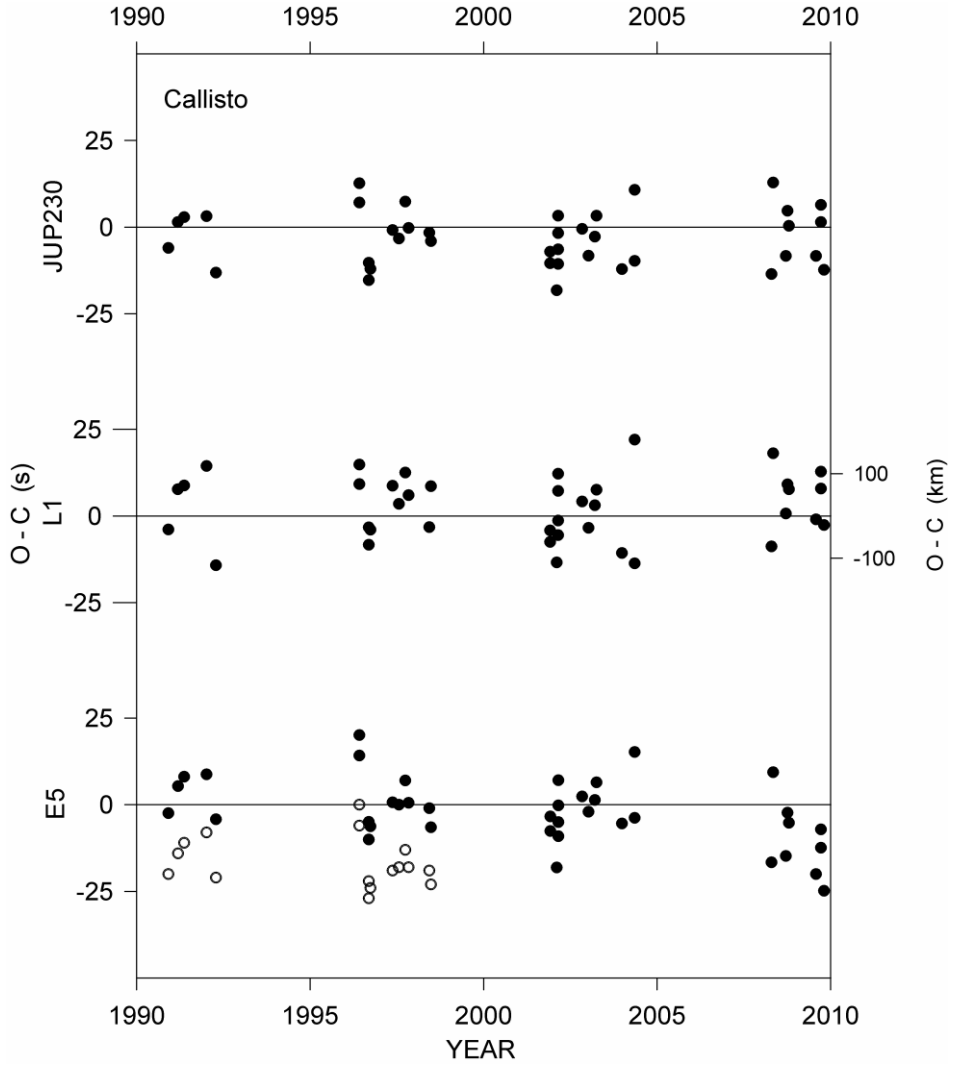

Fig. 13. The O – C residuals for Callisto relative to E5 grow increasingly negative in 2008 and 2009. The open circles represent results from an old BDR model of Callisto reported by Mallama et al., 2000a as discussed in the text.

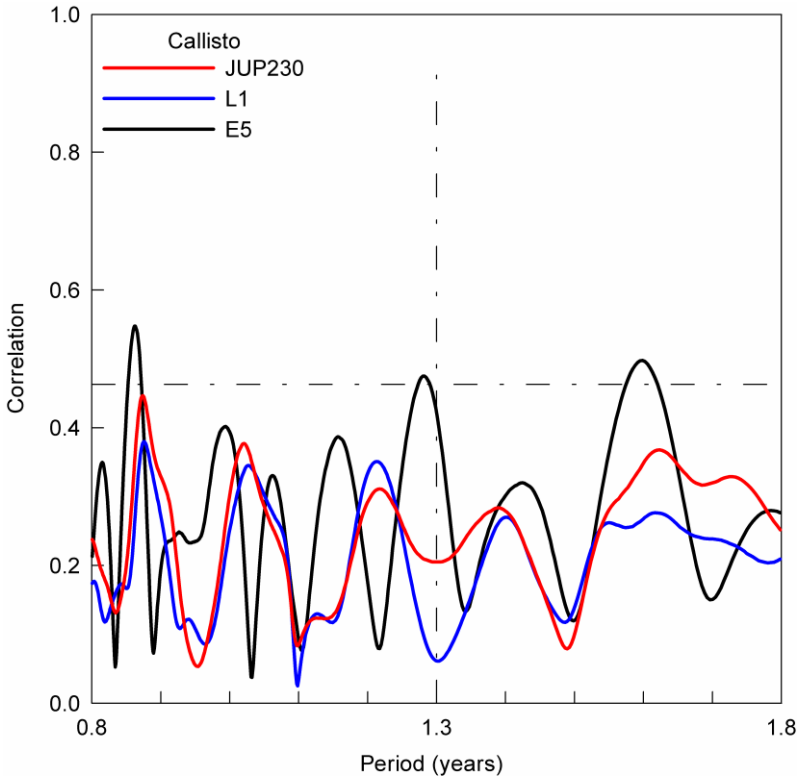

Fig. 14. The correlation function for Callisto and E5 shows only weak evidence for a 1.3 year period relative to E5.

5. Characteristics and interpretation of the oscillations

Mismodeling of the 1.3 year along-track oscillations of Io, Europa and Ganymede is reported in this paper for the first time. Table 3 lists periods, amplitudes and phases for the statistically significant oscillations relative to the three modern ephemerides. The amplitudes are much larger for E5 (4.6 to 15.0 s) than for L1 (1.2 to 3.7) . The oscillations referenced to JUP230 are only significant for Europa and that amplitude is only 1.1 s. The phase for the oscillation of any given satellite relative to L1 and JUP230 is roughly opposite to that for E5. This difference is nearest to π radians in the case of Europa where the phases are determined most accurately. The L1 and JUP230 phases for Europa are almost equal. The oscillations of Ganymede are approximately out of phase to those of Io and Europa for both E5 and L1.

Table 3. O – C oscillations with periods near 1.3 years

	Ephemeris	Period (years)	Amplitude (seconds)	Phase (radians)
Io	E5	1.28 (0.03)	4.6 (0.2)	0.87 (0.04)
	L1	1.31 (0.01)	1.2 (0.2)	4.96 (0.19)
Europa	E5	1.27 (0.02)	15.0 (0.5)	0.90 (0.03)
	L1	1.30 (0.01)	3.6 (0.4)	4.35 (0.09)
	JUP230	1.32 (0.01)	1.1 (0.2)	4.26 (0.16)
Ganymede	E5	1.30 (0.05)	13.8 (1.0)	4.28 (0.06)
	L1	1.25 (0.01)	3.7 (0.8)	1.99 (0.26)

The periods of the oscillations described above are close to those of the resonant perturbations between Io, Europa and Ganymede. Their existence seems to imply that the perturbations are not represented accurately enough in the ephemerides. The π radian phase differences between E5 and the other two ephemerides suggest that the amplitudes of the modeled perturbations are either too large for E5 and too small for L1 and JUP230, or vice-versa. Callisto does not participate in the resonances of the other 3 satellites, so strong sinusoidal O – C variations are not expected.

The dynamical importance of the three bodies in resonance is the associated librations that force orbital eccentricities which, in turn, lead to the dissipation of tidal energy inside the satellites. The effect is most pronounced for innermost Io and accounts for its volcanic activity. Yoder and Peale, 1981 explained this phenomenon and it is summarized by Murray and Dermott, 1999.

6. Estimated uncertainty of the timings

The timings contained in Table 1 are the fundamental observational result of this paper. These data have dynamical and geophysical implications so it is important to know their accuracy. The overall uncertainty of a datum is equal to the square root of the sum of the squares (rss) of the uncertainties of the observationally measured timing and of the modeling of the eclipse.

The observational uncertainty can be estimated from timing differences where one eclipse was recorded by multiple observers. Table 4 shows that the average standard deviation of such differences increases by more than a factor of 3, from 0.80 s for Io to 2.45 s for Callisto. These values are nearly inversely proportional to the satellites velocities, which decrease from 17.3 km/s for Io to 8.2 for Callisto. In the last column of the table the standard deviations of the timings are multiplied by the satellite orbital velocities to convert from times to distances. The much narrower range of distances indicates that orbital velocity alone accounts for most of the variation in observational uncertainty. The average of the standard deviations is 15 km or 4 milli-arc second (mas).

Table 4. Statistics for eclipses timed by multiple observers.

	Eclipses with Multiple Timings		Average of Standard Deviations	
Satellite	Eclipses	Timings	Seconds	Km
Io	36	74	0.80	14
Europa	23	48	0.99	14
Ganymede	33	72	1.21	13
Callisto	6	12	2.45	20

The uncertainty of the model can be approximated by taking the square root of the average of the sums of squares of the delta radius values. That value for the data in Table 2 corresponding with the best fitting ephemeris (JUP230) is 18 km or 5 mas. When the observational and model uncertainties are combined in the rss sense the total uncertainty is 6 mas.

This estimated uncertainty should be less than or equal to the rms values of the O - Cs because the residuals include a component of ephemeris error. When the JUP230 values in Table 2 are converted from units of time to distance they are 28 km or 7 mas for Io, 26 km or 7 mas for Europa, 56 km or 15 mas for Ganymede and 65 or 17 mas for Callisto. Thus the estimated overall uncertainty of 6 mas is validated for Io and Europa. The larger rms residuals for Ganymede and Callisto may indicate that 6 mas is an underestimate of the overall uncertainty for those satellites unless there is significant ephemeris error. The underestimation may be due to their larger physical diameters which increases the difficulty of modeling their BDRs to the same level of accuracy as for Io and Europa. In any case, the overall uncertainty for Ganymede and Callisto must not be greater than about 15 mas.

The high precision of the data and its nearly continuous distribution in time permits very tiny oscillations to be detected. The smallest amplitude in Table 3 is 1.1 +/- 0.2 s for Europa whose orbital velocity is 13.7 km/s. The amplitude in km is 15 +/- 3 which, at the mean distance from Jupiter, corresponds to 3.9 +/- 0.7 mas.

Acknowledgments

This research was supported in part by NASA through the American Astronomical Society's Small Research Grant Program. Robert J. Modic, Donald F. Collins and Maurizio Martinengo supplied observational data in addition to that obtained by the authors. The reviews by Valéry Lainey and an anonymous referee were very helpful, as were comments by Phillip Nicholson, Stanton Peale and Robert Jacobson.

References

Baum, W.A. and Code, A.D. 1953. A photometric observation of the occultation of σ Arietis by Jupiter. *Astron. J.,* **58**, 108-112.

Bevington, P.R. 1969. Data reduction and error analysis for the physical sciences. McGraw-Hill, NY.

Buratti, B. 1991. Ganymede and Callisto: surface textural dichotomies and photometric analysis. *Icarus*, **92**, 312-323.

Jacobson, R., Haw, R., McElrath, T., and Antreasian, P. 1999. A comprehensive orbit reconstruction for the Galileo prime mission in the J2000 system. Presented at AAS/AIAA astrodynamics meeting, Girdwood, Alaska, USA. August 16,1999. Publication number AAS 99-330. http://trs-new.jpl.nasa.gov/dspace/bitstream/2014/17924/1/99-1374.pdf.

Lainey, V., Arlot, J.E., Vienne, A. 2004a. New accurate ephemerides for the Galilean satellites of Jupiter, II. Fitting the observations. *Astron. Astrophys.* **427**, 371-376. doi: 10.1051/0004-6361:20041271.

Lainey, V., Arlot, J.E., Karatekin, Ö, and Van Hoolst, T. 2009. Strong tidal dissipation in Io and Jupiter from astrometric observations. *Nature*, **459**, 957-959. doi:10.1038/nature08108.

Lainey, V., Duriez, L., Vienne, A. 2004b. New accurate ephemerides for the Galilean satellites of Jupiter, I. Numerical integration of elaborated equations of motion. *Astron. Astrophys.* **420**, 1171-1183. doi: 10.1051/0004-6361:20034565.

Lainey, V., Duriez, L., Vienne, A. 2006. Synthetic representation of Galilean satellites' orbital motions from L1 ephemerides. *Astron. Astrophys.* **456**, 783-788. doi: 10.1051/0004-6361:20064941.

Lieske, J.H. 1998. Galilean satellite ephemerides E5. *Astron. Astrophys. Suppl.* **129**, 205-217.

Mallama, A., 1991. Light curve model for the Galilean satellites during jovian eclipse. *Icarus*, **92**, 324-331.

Mallama, A., 1992. CCD photometry for jovian eclipses of the Galilean satellites. *Icarus*, **97**, 298-302.

Mallama, A., Nelson, P., and Park, J., 1995. Detection of very high altitude fallout from the comet Shoemaker-Levy 9 explosions in Jupiter's atmosphere. *J. Geophys. Res*., **100**, 16879-16884.

Mallama, A. and Krobusek, B., 1996. Eclipses of Saturn's moons. *J. Geophys. Res.*, **101**, 16,901-16,904.

Mallama, A., Collins. D.F., Nelson, P., Park, J. and Krobusek, B., 2000a. Precise timings of Galilean satellite eclipses and assessment of the E5 ephemeris. *Icarus*, **147**, 348-352, doi:10.1006/icar.2000.6455.

Mallama, A., Krobusek, B., Collins. D.F., Nelson, P., and Park, J., 2000b. The radius of Jupiter and its polar haze. *Icarus*, **144**, 99-103, doi:10.1006/icar.1999.6276.

Mallama, A., Sôma, M., Sada, P.V., Modic, R.J., and Ellington, C.,K. Astrometry of Iapetus, Ariel, Umbriel, and Titania from eclipses and occultations. *Icarus*, **200**, 265-275, doi:10.1016/j.icarus.2008.11.022.

Murray, C.D. and Dermott, S.F. , Solar System Dynamics. Cambridge University Press, Cambridge, UK. pp. 396-399.

Neugebauer, G., Matthews, K., Nicholson, P.D., Soifer, B.T., Gatley, I. and Beckwith, S.V.W. 2005. Thermal response of Iapetus to an eclipse by Saturn's rings. *Icarus*, **177**, 63–68. doi:10.1016/j.icarus.2005.03.002.

Nicholson, P.D., French, R.G., and Matthews, K. 1997. Eclipses and occultations of Saturn's satellites observed at Palomar in 1995. Paper presented at the 1997 Workshop on Mutual Events and Astrometry of Planetary Satellites, Catania, Italy.

Spencer, J.R., Shure, M. A., Ressler, M.E., Goguen, J.D., Sinton, W.M., Toomey, D.W., Renault, A. and Westfall, J. 1990. Discovery of hotspots on Io using disk-resolved infrared imaging. *Nature* **348**, 618-62I.

Squyers, S.W. and Veverka, J. 1981. Voyager photometry of surface features on Ganymede and Callisto. *Icarus*, **46**, 137-155.

Vasundhara, R., Arlot, J.-E., Lainey, V., and Thuillot, W. 2003. Astrometry from mutual events of the jovian satellites in 1997. *Astron. Astrophys.* **410**, 337-341. doi: 10.1051/0004-6361:20030.

Yoder, C.F. and Peale, S.J. 1981. The tides of Io. *Icarus* **47**, 1-35.

Table 1

Satellite number (1-4), ingress or egress (I/E), and seconds after the epoch of J2000

2I -289105670.6
1I -288239185.5
4I -286773407.0
3E -278930708.0
4E -278072095.2
2E -277121540.1
1E -276762150.5
1E -275997505.5
4E -272282254.2
4I -252037849.1
1I -251693173.4
3E -245498726.4
2E -245493991.6
2E -244879956.1
3E -244879625.0
1E -243427504.2
4E -243340500.3
1E -242815797.6
2E -242730782.0
2E -242730779.2
3E -241783903.3
3E -241783901.2
3I -241177178.3
1E -240827738.6
2I -223087969.4
1I -218511302.8
1I -218511299.9
2I -218482024.9
3I -217651226.5
2I -216946805.6
3E -209592901.2
1E -208411138.8
1E -208258216.8
1E -208258216.4
3I -207745330.4
3E -207735501.6
3I -206507032.4
2E -206498707.1
3E -206497321.9
1E -206270151.5
1E -203823300.7
1I -189304643.1
2I -187470101.4
1I -187469931.7
1I -185329455.1
1I -185329457.1
1I -184870778.8
2I -183785292.0
2I -183171161.0
1E -175076929.6
2E -174564911.2
2E -174564912.0
1E -174006451.5
1E -173241819.7
3I -173075383.9
3E -173067908.5
1E -172630103.7
1E -171253739.3
3I -168741228.1
3E -150779918.6
1I -150006986.2
2I -149395912.3
2I -149395909.0
1I -149395410.5
1I -149395409.2

```
1E -140518839.1
2E -140174018.7
1E -139142513.1
1E -139142515.1
3I -138405858.9
2E -138331502.1
1E -138072015.3
3I -136548404.1
3E -133443418.1
3I -119212965.8
1I -119118128.4
2I -117769250.2
2I -116541003.1
3E -116106840.7
1I -115448573.2
2I -115005618.0
1I -114836980.2
2I -114391457.0
1I -114378280.1
4I -113107430.5
4I -113107424.3
3I -113022168.0
2E -106703478.8
2E -106396330.3
2E -105782085.8
1E -104583707.2
4E -104411162.8
4E -104411168.1
1E -103971994.9
2E -103632267.9
1E -103513208.5
1E -103207350.7
4E -102963262.1
1E -101219246.5
1E -101219247.6
3E -100007368.3
3E -100007364.7
1I  -85170774.2
3E  -83907724.9
3E  -83907723.5
1I  -83641713.2
4E  -82695037.0
3I  -82063306.2
3E  -82050257.6
2I  -81227573.8
2I  -81227571.5
2I  -79999258.6
2I  -79077971.9
1I  -78442939.8
4I  -76921953.2
3E  -73381451.5
1E  -72012214.4
2E  -72003546.7
1E  -71400513.7
4E  -71113404.0
1E  -70788806.4
1E  -70330022.1
3E  -70285069.2
3E  -70285070.5
1E  -70024170.0
1E  -69718316.8
1E  -68953663.7
1E  -68647800.8
4E  -68217716.5
2E  -67396362.2
2E  -64325162.3
2E  -64325166.0
2I  -50210731.0
3I  -49862192.6
4E  -49397593.8
4I  -47962493.4
```

```
1I  -45717768.9
1I  -45717769.9
1I  -44341570.3
1I  -43729915.3
2I  -43148144.2
2I  -43148140.5
3I  -43050600.7
3I  -42431311.8
1E  -38216747.0
2E  -37609830.0
1E  -37605049.0
1E  -37605049.4
1E  -37452124.0
3E  -36846096.7
1E  -36840417.5
3I  -36238200.7
3E  -36226830.7
2E  -36074035.8
2E  -35459715.4
1E  -33475973.9
1E  -33475976.1
2E  -33309530.0
3E  -29414644.1
2I  -13665690.6
3I  -13323250.9
3E  -13314401.2
1I  -13145086.3
1I  -11768867.1
1I  -10545557.7
2I  -10288151.0
3E  -10218353.8
3I   -9607609.7
3I   -9607611.5
3E   -9599169.9
3E   -9599167.9
1I   -9016409.9
1I   -9016408.1
1I   -9016411.0
2I   -8138616.0
2E   -3829752.9
1E   -3656353.7
1E   -3503430.2
3E   -3406758.0
1E   -2891724.1
3I   -2795253.4
3I   -2795245.3
3E   -2787460.4
3E   -2787463.2
2E   -2293956.2
1E   -2280014.0
2E   -1679626.2
2E     470546.0
1E     472715.7
1E     472715.1
2E    1084895.4
2E    3849466.3
3I    4017448.5
3E    4024745.9
3E    4024745.2
1I   19427370.3
2I   20115663.4
3I   20118532.8
2I   22878834.6
1I   23403089.8
2I   23492884.1
3I   23833772.5
3E   23841028.6
3E   23841028.1
1I   24167650.2
1I   24779307.1
2I   25028041.8
```

```
1I   25390964.3
2I   25642128.6
2I   26256225.7
3E   30652819.4
1E   31515674.6
1E   31668604.5
2E   31793336.7
2E   32100455.7
2E   32714740.8
1E   33656674.9
1E   33656672.4
3I   33741330.4
3I   33741325.9
3I   33741329.5
3E   33749324.9
3E   33749323.7
1E   34268392.5
1E   34268390.9
2E   34864837.3
3I   37456855.1
3I   37456853.5
3I   37456853.7
3E   37465206.9
3E   37465210.2
3E   37465212.1
2E   37629299.6
2E   37629298.6
1E   37632836.4
1E   37632836.8
2E   38243630.5
2E   38243632.6
1E   38244548.4
1E   38244550.2
2I   51746539.3
2I   51746536.6
3I   53555774.1
2I   53895683.9
1I   53986999.3
2I   54509709.6
2I   54509708.3
1I   55974808.3
2I   56658738.7
2I   56658739.2
3E   56661797.4
3E   56661794.2
3E   56661793.1
1I   58421345.1
1I   58727163.7
2I   58807763.5
1I   59338805.2
1I   59338805.5
2I   59421777.0
4I   60631889.4
4I   60631885.7
3E   64711564.9
1E   66228322.3
4I   66420804.9
2E   66493961.5
2E   66493965.8
3E   66569329.5
3E   66569325.5
3E   66569321.5
1E   66840030.6
3E   67188557.6
3I   67796308.1
3I   67796307.5
4I   67868208.8
4I   67868204.3
4E   67880251.7
4E   67880246.3
1E   68216381.5
```

```
1E   68216382.1
1E   68216383.2
3E   68427029.3
2E   68643711.1
1E   70204444.7
1E   72192494.4
2E   74786443.7
2E   74786443.8
2E   74786444.4
4E   89595031.8
3I   91323689.0
1I   92521340.9
1I   93285866.3
3I   94419130.7
2I   94428158.1
4I   95366668.3
1E  100022499.2
2E  100271893.2
2E  100271892.1
3E  100623831.2
3E  100623829.8
2E  100885995.9
1E  101092982.5
4E  101173634.9
1E  101857609.6
1E  102010537.4
4E  102621051.6
3E  104338917.4
1E  104763225.2
3I  104944887.1
1I  121728064.5
2I  122678959.5
2I  122678957.1
3E  124150095.1
4E  125775078.0
2E  134662727.1
2E  134662729.1
3E  134674328.2
3E  134674329.4
2E  135276777.6
1E  136415587.5
1E  136415587.7
2E  136504894.1
1E  136568508.6
1E  136568508.7
1E  137180219.6
4I  137339438.1
4E  137350242.5
2E  137426009.0
2E  137426008.4
1E  137638999.4
3E  137769928.2
3E  137769931.4
1E  138097780.5
1E  138403636.2
1E  138403632.9
1E  138556565.9
3E  139008250.0
1E  139015343.8
2E  139268282.6
3I  139615469.5
3I  139615473.2
1E  139779979.1
1E  139932901.5
1E  140085831.5
2E  140189449.0
1E  140391680.3
2E  140803566.3
2E  141724752.5
1I  159343946.4
1I  160872899.6
```

3I 161902935.3
2I 161981521.4
2I 163823714.9
2E 168745771.4
1E 168832179.2
1E 168832175.8
2E 169052791.9
1E 169138021.8
1E 169596792.2
1E 169596793.8
1E 170514350.1
1E 170514347.9
1E 171584834.0
1E 171584833.6
2E 171816018.2
3E 171817971.5
1E 172961191.5
2E 173044140.4
2E 173044141.2
3I 173047427.8
3I 173047425.9
3E 173056272.2
3E 173056267.1
2E 174579307.8
1E 174949249.4
3I 176762445.3
3I 176762446.6
1I 191455557.8
2I 191458173.5
3E 191628102.9
2I 193607642.5
1I 194666292.9
1I 194819184.5
2I 196064177.3
3I 196573160.1
3I 196573160.7
1I 196653934.9
1I 196653935.8
2I 196985387.9
3I 197192206.3
2E 202521634.5
2E 202828683.4
2E 203135733.1
3E 205247437.0
2E 205592102.0
3I 205859880.5
2E 205899143.6
1E 206142477.5
3E 206485774.4
1E 206754191.5
1E 206754191.0
1E 207060050.5
1E 207518839.9
1E 207518835.2
1E 207671772.8
1E 208130556.8
1E 208130553.8
2E 208355468.6
1E 208742276.8
3E 208962443.5
1E 209048137.1
1E 209506927.2
1E 210118644.8
2E 210197684.7
3E 210200750.6
3I 210813227.7
1E 211494997.4
3I 229385613.2
3I 230004613.8
3E 230012399.4
2I 230761079.2

2I 231989419.0
1I 232435185.2
2I 232603592.8
2E 236298019.0
1E 236724593.6
3E 236822895.3
2E 237219299.2
2E 237219297.8
1E 237336276.5
1E 237336278.1
1E 237489200.6
2E 237526376.8
2E 237833472.0
1E 238253817.7
1E 238559668.7
1E 238559668.2
1E 238712593.7
1E 238865518.7
2E 239061809.3
3I 239290996.0
3I 239290994.1
3I 239290997.0
2E 239675976.0
1E 240241865.0
1E 240700648.5
3I 241148506.5
1E 241312369.1
1E 241924090.9
2E 242439625.7
2E 242439629.8
1E 243300476.7
1E 243300479.1
1E 243606341.5
3I 244244302.4
2E 244589046.9
2E 244589045.8
1E 244676863.8
1I 258278488.6
1I 260266185.1
4E 261806705.1
2I 262080974.3
2I 262080973.8
1I 262253860.9
2I 262388029.1
3I 262817867.9
4I 263243583.5
3E 264067243.8
1I 264394441.3
3I 264675083.9
2I 264844688.4
1I 265617644.7
3E 270258941.6
3E 272735911.3
1E 272812718.1
2E 272839661.8
2E 272839659.1
1E 273118570.2
1E 273118571.3
1E 273271495.7
1E 273271497.6
2E 273761039.1
1E 273883204.2
3I 273962288.2
3I 273962285.5
3E 273974362.2
3E 273974362.1
1E 274189061.3
3I 274581507.9
3I 274581507.9
1E 274800775.6
4E 274836568.9

```
1E  275259569.4
2E  275603723.9
2E  276217937.9
4I  276269342.2
3I  276439218.3
3I  276439221.9
1E  276483017.9
1E  276483019.3
2E  276525034.1
3I  277677641.5
3E  277689981.0
3E  277689986.2
4E  277732333.6
1E  277859408.8
1E  279235808.3
1E  279235810.0
1I  292225927.9
1I  292837563.5
1I  292837561.6
2I  293095763.1
2I  296166289.2
2I  296166290.9
2I  296166288.1
3I  296253575.2
3I  296253576.1
1I  296813117.5
1I  297118924.0
3I  297491953.7
3I  298111110.3
1I  298953782.1
1I  298953781.1
1I  300177027.6
1I  300329936.9
1I  300482840.5
2I  300772550.9
2I  301079682.8
2I  301079682.6
4I  302326081.3
3E  306174021.1
1E  306301871.1
4E  306686709.7
4E  306686714.6
2E  307540067.8
1E  307678195.6
1E  309054549.9
3E  309270335.9
4I  309565798.6
3I  309876535.0
2E  309997237.1
2E  310918670.5
1E  311042657.0
3E  311128216.4
3E  311128216.2
3I  311734451.4
1E  312113184.6
1E  312419052.3
3E  312986035.8
```